Nanocatalysts: Properties and applications

Gaikwad, A.V.

Publication date
2009

Chapter 2

Section A

In-Situ UV-visible study of Pd nanocluster formation in solution

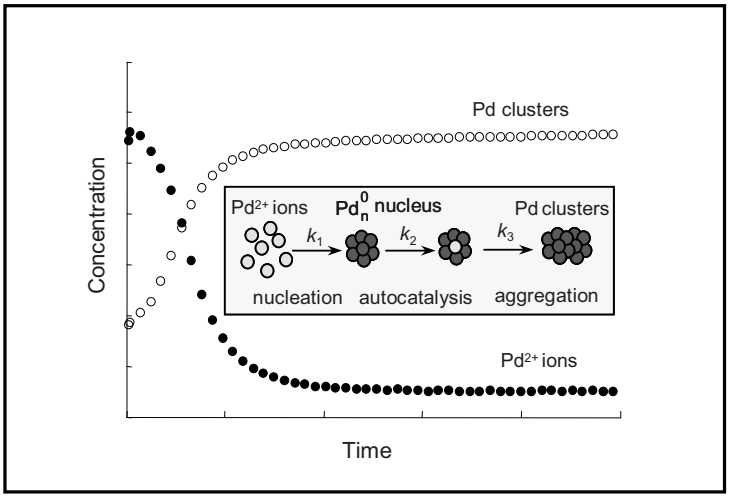

Part of this work is published as "In Situ UV-visible Study of Pd Nanocluster Formation in Solution", A. V. Gaikwad and G. Rothenberg, *Phys. Chem. Chem. Phys.*, **2006**, *8*, 3669.

Introduction

Palladium is perhaps the most important and certainly one of the most versatile of the transition metals in catalysis applications. A large amount of data was gathered in the past five decades on the activity and selectivity of Pd catalysts, with applications in oxidation chemistry (including fuel cells[1]), hydrogenation,[2] and C–C coupling reactions.[3] Most of the studies focus either on homogeneous (Pd-ligand) complexes or on heterogeneous (supported) Pd crystallites. However, palladium nanoclusters are emerging as key players in many of these systems.[4-8]

Given the almost ubiquitous presence of Pd nanoclusters in Pd-catalysed systems, it is surprising that we know little about how these clusters actually form in solution, and what role they play in the catalytic cycles.[9] The reason is that quantifying the transition metal clusters' properties *in situ* is difficult. Transmission electron microscopy (TEM), energy dispersive x-ray analysis (EDX), and other *ex situ* methods give us valuable information on the clusters' size, shape, and composition after the reaction.[10, 11] However, this information does not tell us how the clusters formed, nor how they function in solution. It is also possible to measure the clusters' electronic spectra *in situ*. The shape, size, and surface composition of a colloidal metal particles determine the absorption in the UV-visible range.[7] The idea of monitoring nanocluster formation using UV spectroscopy was originally proposed by Reetz and Maase[12] Typically, electronic spectra of nanoclusters show absorption bands due to the excitation of the plasmon resonance.[13, 14] These bands can be correlated to physical properties using theoretical treatments such as Mie theory.[15] Metals that give a distinct plasmon peak, such as Au, Ag ,Cu and Co, are relatively easy to monitor.[16-18] The problem is that many transition metals do not show distinct surface plasmon peaks, and the presence of metal ions, clusters, and stabilising agent gives a plethora of spectra that is difficult to untangle.[19]

A second problem is fitting a mechanism and a kinetic model to the data. Some reports recently proposed a new mechanism of cluster formation.[20-24] This mechanism features a slow continuous nucleation step, followed by fast autocatalytic surface growth and bimolecular agglomerative growth.[23] Recently, we presented a multivariate approach to extract the clusters' contribution to the spectra. By combining net analyte signal (NAS) and principal components analysis (PCA) methods, we obtained quantitative and qualitative kinetic profiles for the ion reduction process.[25] In this chapter we use the same NAS/PCA approach to extract the reduction and clustering profiles in Pd systems. We synthesize various palladium clusters using different precursors such as $PdCl_2$, $Pd(OAc)_2$,

and $Pd(NO_3)_2$ and various tetra-*n*-octylammonium carboxylates as reducing and stabilising agents. The UV-visible results are validated using transmission electron microscopy. We then apply a derivative of three step model and simulate the clustering kinetics. This kinetic model correlates well with the experimental data. Our results show that the counteranions play a crucial role in the cluster stabilisation.[26]

Experimental

Materials and instrumentation. *In situ* UV-visible measurements were performed using a Hewlett Packard 8453 spectrophotometer with a diode array detector. The quartz cuvette (Hellma Benelux, approximately 3.5 mL, path length 1 cm) was mounted on a sample holder with controlled heating (Neslab constant temperature bath) and stirring (compressed air was used to turn the stirrer under the cuvette). The recorded wavelength range was 190–1100 nm, at 1 nm resolution. TEM images were obtained with a JEOL model JEM-1200 EXII instrument, operated at an accelerating voltage of 120 kV. Unless stated otherwise, chemicals were purchased from commercial firms (>98% pure) and used as received. All solvents were degassed for 10 min with dry N_2 prior to use. Stock solutions of tetra-*n*-octylammonium formate (TOAF), tetra-*n*-octylammonium glycolate (TOAG), and tetra-*n*-octylammonium acetate (TOAA) were prepared according to a previously published procedure.[27] Stock solutions (10 mM) of Pd^{2+} ions were prepared by dissolving 17.7 mg of $PdCl_2$ or 23.0 mg of $Pd(NO_3)_2$ or 22.4 mg of $Pd(OAc)_2$ in 10.00 ml of DMF (99.8%). Data analysis routines for NAS, PCA, and the kinetic models were programmed in Matlab.[28]

Preparation of tetra-*n*-octylammonium carboxylates. *Example: tetra-n-octylammonium formate (TOAF)*. This is a modification of the procedure reported by Reetz and Maase.[12] 40 g of ion exchange resin (Amberlite IRA 402, Cl^- form) suspended in a 1.5 M NaOH solution were charged to a column that was subsequently flushed with 3 L of 1.5 M NaOH. A slight N_2 overpressure was applied. The elute was tested for Cl^- using $AgNO_3$. The colour of the resin changed from yellow (Cl^- form) to orange (OH^- form). The column was then flushed with 3 L of distilled water followed by 500 mL of 0.2 M formic acid solution. This was followed by 3 L distilled water and finally 1 L MeOH, switching to an organic medium. The resin was left to swell for 1 h and the column was subsequently flushed with an 18 mM solution of tetra-*n*-octylammonium bromide (TOAB) in MeOH, until the elute tested positive for Br^- using $AgNO_3$. The MeOH was evaporated on a rotavapor and the crude TOAF (light oil) was dried for 24 h under vacuum.

TOAA and TOAG were similarly prepared, using acetic acid and glycolic acid in place of formic acid.

Procedure for preparing Pd cluster calibration samples. A Schlenk-type glass vessel equipped with a rubber septum and a magnetic stirrer was evacuated and refilled with N_2. The vessel was then charged with 20 ml of 0.5 mM $PdCl_2$/DMF solution. This vessel was stirred and heated at 65 °C for 1 h. Then, 0.5 ml of 100 mM of TOAF/DMF was added in one portion into the vessel and the reaction was continued for 24 h. DMF was then evaporated at 65 °C and 250 mm Hg. The dry clusters were weighed and then redispersed in 25 ml of DMF.

Procedure for *in situ* monitoring of Pd cluster formation. *Example: $PdCl_2$ precursor*. The UV-Visible spectrum of blank sample of $PdCl_2$/DMF (0.5 mM) solution (2 ml) was first measured. This was used as a calibration sample for Pd^{2+} ions. Then, TOAF (50 µl, 100 mM) was added to the cuvette in one portion. The reaction mixture was stirred and heated at 65 °C. UV/Vis spectra were recorded every 1.1 min for 60 min. This data was processed using NAS/PCA techniques, giving the reaction profiles for the initial reduction process. Reproducibility was validated in triplicate experiments.

The same procedure was used for monitoring the Pd nanocluster formation using $Pd(NO_3)_2$ and $Pd(OAc)_2$ precursors in combination with the reducing agents TOAA, and TOAG, respectively.

Results and Discussion

Cluster synthesis and spectroscopic measurements. The palladium clusters were synthesised in solution using the salt reduction method.[29, 30] All the reactions were performed in degassed solvents and under an inert atmosphere. In a typical reaction (eq 1), the Pd salt precursor was first dissolved in N,N,dimethylformamide (DMF) and subsequently reduced by excess amount of tetraoctylammonium carboxylate salt (4–5 equivalents), that also functions as a stabiliser.[12] The stoichiometry was described by Bönnemann and Richards[31] using eq 1, where the Pd_n^0 cluster is stabilised by the tetraoctyl ammonium chloride species (the case of TOAF is more complicated, as hydrogen can also in principle form via the formate⇔bicarbonate equilibrium[32]). Reaction progress was monitored by UV-visible spectrometry (Figure 1). We did not observe any bulk metal precipitation that may affect the UV-visible properties of nanoclusters.

$$nPdCl_2 + 2n[RCOO^-][Oct_4N^+] \rightarrow Pd_n^0 + nR - R + 2nCO_2 + 2n[Oct_4N^+][Cl^-] \quad (1)$$

Figure 1 shows the time resolved spectra for Pd cluster formation. Pure $PdCl_2$ in DMF shows a maximum at 420 nm. As the reaction proceeds, Pd^{2+} ions are reduced to Pd° atoms and further grow to form clusters. This transition decreases the absorbance at 420 nm.

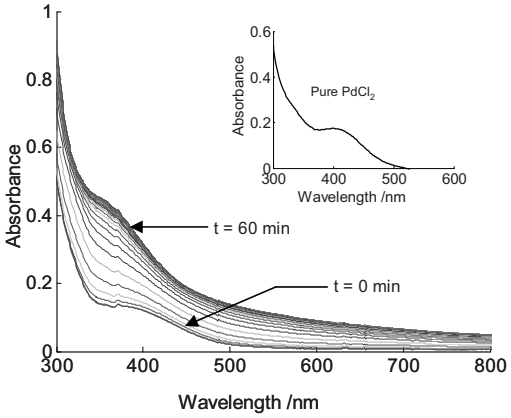

Figure 1 (colour available in online version). Time-resolved UV-visible spectra during the reduction of Pd^{2+} ions with tetraoctylammonium formate (TOAF) in DMF. The inset shows the spectrum of pure $PdCl_2$ in DMF. Reaction conditions: $PdCl_2$ (2 mL, 0.5 mM), TOAF (0.05 mL, 100 mM), 65 °C, dry N_2 atmosphere, magnetic stirring.

Metal nanoparticles absorb photons in the UV-visible region due to a coherent oscillation of the conduction band electrons induced by the interacting electro-magnetic fields. These resonances are known as surface plasmons.[33, 34] Several transition metals, including Pd, do not show pronounced surface plasmon peaks due to *d–d* interband transitions.[35, 36] In our case, we observed the broad shoulder around 370–390 nm corresponds to the formation of Pd nanoclusters.[15, 37] Using transmission electron microscopy (TEM) we found that the above synthesis procedure gives ~3 nm clusters (Figure 2). The size distribution was ± 1.0 nm (> 75 % of the total particles counted were in 2–3 nm range). The 'tail' in the size distribution graph is a consequence of the particle counting algorithm.[38] This is in good agreement with the results observed by Reetz and co-workers.[12, 39]

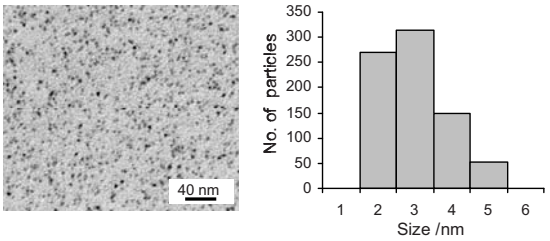

Figure 2. Transmission electron micrograph (left) and corresponding size distribution of Pd clusters prepared by reducing $PdCl_2$ with TOAF. The Histogram for the size distribution is based on 800 particles counted.

Extracting the concentration profiles from the raw spectra. Time-resolved spectroscopic measurements generate large amounts of data. The spectrum contains all the physical information about all of the absorbing species in the mixture, but extracting this information is not trivial. Here we used a multivariate calibration model (the net analyte signal or NAS approach) to isolate the contribution of the various absorbing species. Pd clusters absorb in across a wide range of wavelengths (see Figure 1) but do not show a clear absorption maximum. Thus, choosing a particular wavelength for following the cluster formation is difficult. The NAS approach provides a simple way for isolating the clusters contribution to the spectra. It requires a minimum of two spectra of the analyte of interest, plus spectra of mixtures that contain only the interferents. One then calculates the orthogonal projection of the vector that represents only the spectrum of the analyte on the space spanned by the vectors representing the interferents.[40] From this NAS vector one calculates the analyte concentration (a detailed description of this method is given elsewhere[25, 41]). Using this method, we obtain the cumulative spectra of all of the known analytes, and a remaining residual signal (Figure 3). PCA analysis on this residual signal shows that > 90% of it is explained by introducing just one artificial species (continuous curve in Figure 3). This indicates that the nanoclusters contain one main type of UV-visible active species.

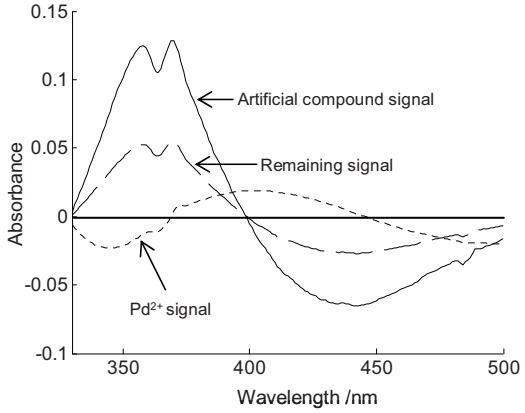

Figure 3. NAS/PCA approach showing the Pd^{2+} signal (dotted curve), the calculated signal for the one artificial compound (continuous curve) and the remaining signal (dashed curve).

In our case, the analytes are Pd^{2+} cations and Pd clusters, and the interferents are the solvent (DMF) and the reducing/stabilising agents. The Pd^{2+} solution was calibrated using known concentrations of PdX_2 (X = Cl^-, NO_3^-, AcO^-). The Pd cluster calibration solutions were prepared by synthesising the clusters as organosols in DMF using Reetz's method.[12, 42] Although we do not know the clusters' molecular weight, we know the initial weight of the Pd and tetra-*n*-octylammonium carboxylate salts. By subtracting the absorption spectra of the stabilizer and a uniform particle size (*vide infra*), we obtain particles with a similar spectrum to that of the calibration samples (see figure 6). The resulting spectra represent the Pd clusters. Using the NAS approach, we managed to obtain, for the first time, quantitative concentration profiles for *both* the Pd^{2+} ions and the Pd clusters (Figure 4).

Constructing a full calibration model is a lot of work.[43] Therefore, a key question is whether one may use the calibration samples from one system in another, similar system. We examined the reduction and clustering profiles, using $PdCl_2$ as cluster precursor and tetraoctylammonium formate (TOAF) as reducing agent/stabiliser. These profiles were quantified using two calibration models: One based on cluster calibration samples prepared using TOAF, and another based on cluster calibration samples prepared using tetraoctylammonium glycolate (TOAG). As Figure 5 shows, the 'similar' calibration model gives a biased profile, with a deviation of *ca.* 25%. This means that clusters

prepared using TOAG and TOAF differ significantly in their size and/or shape (note that both the concentrations and the number of the calibration samples in both cases were identical).

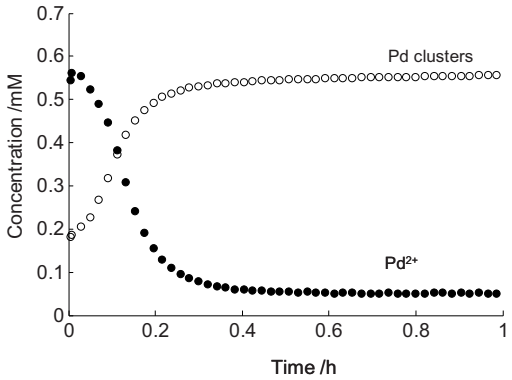

Figure 4. Concentration profiles showing the reduction of $PdCl_2$ ('●' symbols) and the formation of Pd clusters ('○' symbols) using TOAF as the reducing agent. Reaction conditions are as in Figure 1.

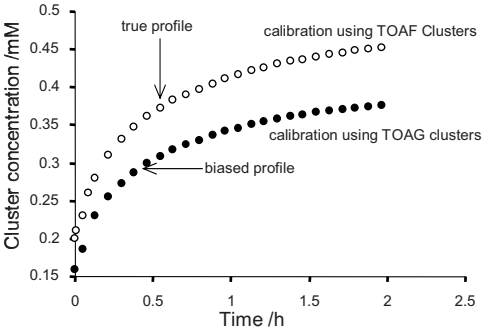

Figure 5. Concentration profiles showing the formation of Pd clusters from the reduction of $Pd(OAc)_2$ with TOAF, obtained by using different cluster calibration samples. '○' symbols denote calibration samples prepared using TOAF and '●' symbols denote cluster calibration samples prepared using TOAG. Reaction conditions: $PdCl_2$ (20 mL of 0.5 mM), TOAF & TOAG (0.5 mL of 100 mM), 65 °C, dry N_2 atmosphere, magnetic stirring.

To understand this difference, let us consider for example the two spectra of Pd clusters prepared using equal concentrations of $PdCl_2$ and either TOAF (Figure 6, solid curve) or TOAG (Figure 6, broken curve). The differences between these spectra reflect

the change in the plasmon resonance, which depends strongly on the cluster concentration and geometry.[15] TOAF is a stronger reducing agent than TOAG. This means that the reaction $Pd^{2+} + 2e^{-} \rightarrow Pd^{0}$ is faster with TOAF, yielding a large number of relatively small clusters (*cf.* Wilcoxon *et al.* for the correlation between the size and the colour of Au clusters[44]). Furthermore, the cluster calibration solutions prepared using different precursors yielded different absorption spectra. Thus, one must use cluster calibration solutions prepared using the same Pd precursor and the same reducing agent.

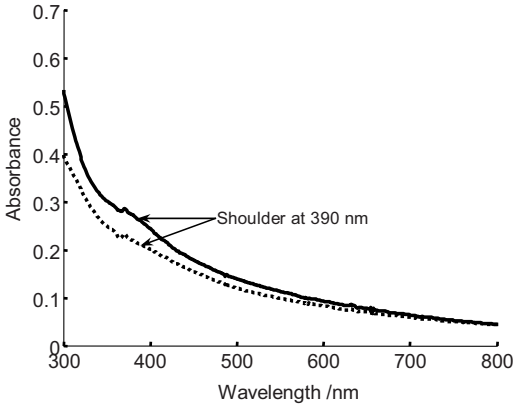

Figure 6. Absorption of Pd cluster calibration solutions prepared from $PdCl_2$ and either TOAF (solid curve) or TOAG (dotted curve) as reducing/stabilising agent. Conditions are the same as for Figure 5.

Reduction, nucleation and clustering kinetics. To find the rate constants of the elementary reactions involved, we fitted a series of kinetic models to the experimental reaction profiles. In principle, the system includes three reactions: ion reduction, nucleation, and cluster formation. We used a similar approach that was reported in the case of Pt clusters.[23] The simplest model uses two equations to describe the ion reduction and cluster growth via autocatalysis (eqs 2 and 3). This gives a two-parameter model, with k_1 and k_2. A more complex model includes also an aggregation step (eq 4), with k_3 as an extra parameter (the Pt model also includes a fourth step, leading to the formation of Pt black, but we did not observe any Pd black in this system owing to the excellent stabilisation by the ammonium salts). In both cases, the first step is a slow continuous nucleation to give the so-called 'critical nucleus', Pd_n^0, followed by fast autocatalytic surface growth. The autocatalytic growth consumes the available Pd^{2+} ions, shutting off the nucleation step and separating nucleation and growth in time.[23]

$$nPd^{2+} + 2ne^- \xrightarrow{k_1} Pd_n^o \quad (2)$$

$$Pd_n^o + Pd^{2+} + 2e^- \xrightarrow{k_2} Pd_{n+1}^o \quad (3)$$

$$Pd_n^o + Pd_m^o \xrightarrow{k3} Pd_{n+m}^o \quad (4)$$

The model was built with the following assumptions: *(i)* an excess of ammonium salt is present, *(ii)* for a given reducing agent, $k_{\text{reduction}} >> k_{\text{nucleation}}$, so that the reduction and the nucleation are considered as one step, with $k_1 = k_{\text{nucleation}}$; *(iii)* the scaling factor for the cluster shell growth is dismissed (this does not affect the model's performance, only the absolute values of the rate constants[45]); *(iv)* in the aggregation step, $n = m$; and *(v)* the nucleation is approximated as a first-order process. The model is then written as in eqs 5–7, where, $[Pd^{2+}]_{t=0} = [Pd_n^0]_{t=\infty} = [Pd^{2+}]_t + [Pd_n^0]_t$

$$-\frac{d[Pd^{2+}]}{dt} = k_1[Pd^{2+}] \quad (5)$$

$$-\frac{d[Pd^{2+}]}{dt} = k_2[Pd^{2+}][Pd_n^0] \quad (6)$$

$$-\frac{d[Pd_n^0]}{dt} = k_3[Pd_n^0]^2 \quad (7)$$

Assumption *(v)* reflects the system's complexity. In a separate series of reactions, we followed the Pd^{2+} conversion in the presence of TOAA for initial $PdCl_2$ concentrations of 0.25 mM, 0.37 mM, 0.50 mM, and 0.75 mM. Our aim was to find the nucleation reaction order but the k_{obs} values were 3.8 h^{-1}, 5.0 h^{-1}, 4.2 h^{-1} and 4.0 h^{-1}, respectively. The problem is that here both the stabilizer and the reducing agent are the same compound, with two effects playing against each other. Thus, we cannot say when the reduction 'stops' and the nucleation 'starts'. We can only obtain via the model an overall picture of the system.

Let us now consider the formation of Pd clusters using $PdCl_2$ and different reducing agents (tetraoctyl ammonium formate TOAF, tetraoctyl ammonium acetate TOAA, and tetraoctyl ammonium glycolate TOAG). The experiments all gave typical S-shaped profiles with a short induction period (note that the spectra were measured simultaneously with the addition of the reducing agent, so this induction period is not an instrumental lag). This induction period is the time required for forming the critical nuclei, which indirectly also depends on the $Pd^{2+} \rightarrow Pd^0$ reduction rate.

Figure 7, top, shows the experimental profiles together with the two-step model results. The fit is excellent in the case of TOAF. This means that there is almost no aggregation, and indeed fits with the very small clusters observed by TEM (3–4 nm). This is not the case for TOAA and TOAG. However, by adding the aggregation step (Figure 7, bottom), we obtain a very good fit also for these salts.

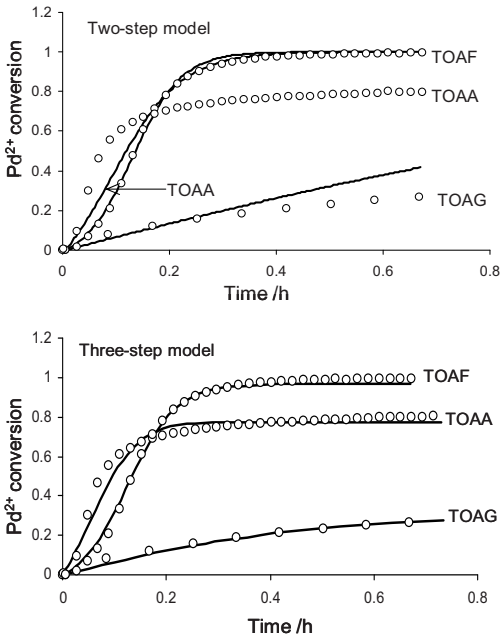

Figure 7. Experimental conversion profiles of Pd^{2+} ions ('○' symbols, all measurements were performed in triplicate), using $PdCl_2$ as precursor and different reducing agents: TOAF, TOAA, and TOAG, and the respective simulated profiles (continuous curves) obtained from the two-step model (top) and the three-step model (bottom). Reaction conditions: 2 mL of 0.5 mM of $PdCl_2$, 0.05 mL of 100 mM of reducing agent, 65 °C, dry N_2 atmosphere, magnetic stirring.

Table 1 gives the corresponding rate constants for the different reducing/stabilising agents. The nucleation rate constant k_1 TOAA is quite higher than TOAF and TOAG. Reetz and Maase showed that the reduction rate increases with the electron-donating capacity of the carboxylate ion.[12] The corresponding pK_a values are 4.75 for TOAA and 3.83 for TOAG (the lower k_1 value in the case of TOAF may reflect the different reduction mechanism *via* hydride transfer). Comparing the k_3/k_2 ratio helps to understand the extent of the aggregation. This ratio decreases in order of TOAG (12.5) > TOAA (0.38) > TOAF

(0.03). Thus, one would expect larger clusters when using TOAG. These results are in good agreement with the extensive TEM studies published by Reetz and co-workers.[12, 39]

Table 1. Model rate constants for $PdCl_2$ and different reducing/stabilising reagents.

Reagents	k_1 (h^{-1})	k_2 (10^4 $M^{-1}h^{-1}$)	k_3 (10^4 $M^{-1}h^{-1}$)	Nanocluster size (nm)[a]
TOAF	1.20	4.10	0.15	1.6
TOAA	4.00	3.30	1.25	2.5
TOAG	0.70	0.10	1.25	5.0 (11.0[b])

[a] The cluster sizes are given for comparison from the extensive TEM studies performed by Reetz and co-workers.[12, 39]

[b] TEM analysis of a $Pd(NO_3)_2$ sample (figure not shown) that was reduced by TOAG showed clusters of 11 nm ± 1.0 nm. The difference reflects the importance of the both the precursor and the reducing agent.

The role of anions and stabilisers. The reduction and clustering profiles can also give valuable information on the role played by the counterions (Cl^-, AcO^-, NO_3^-). In 'wet chemical' cluster synthesis, stabilisation is determined by electrostatic and steric factors.[26] Anions from the precursor salts and reducing agents can adsorb on the cluster surface, forming an electric double layer as shown by Bönnemann and coworkers.[46] Colloidal suspensions stabilised by electrostatic repulsion are sensitive to disruptions of this double layer.[47, 48] Earlier studies showed that metal clusters have a δ^+ surface charge that is countered by anion adsorption.[26] To understand the counterion effects on the aggregation process, we ran a series of experiments using $PdCl_2$, $Pd(OAc)_2$, and $Pd(NO_3)_2$ as precursors and TOAF as reducing/stabilising agent. We monitored the kinetics using UV-visible spectroscopy, and applied the two-step and three-step kinetic schemes as explained above (Figure 8). $PdCl_2$ and $Pd(OAc)_2$ gave a reasonable fit with both models, but $Pd(NO_3)_2$ did not (Figure 8, bottom, the *k*-values are given in Table 2).

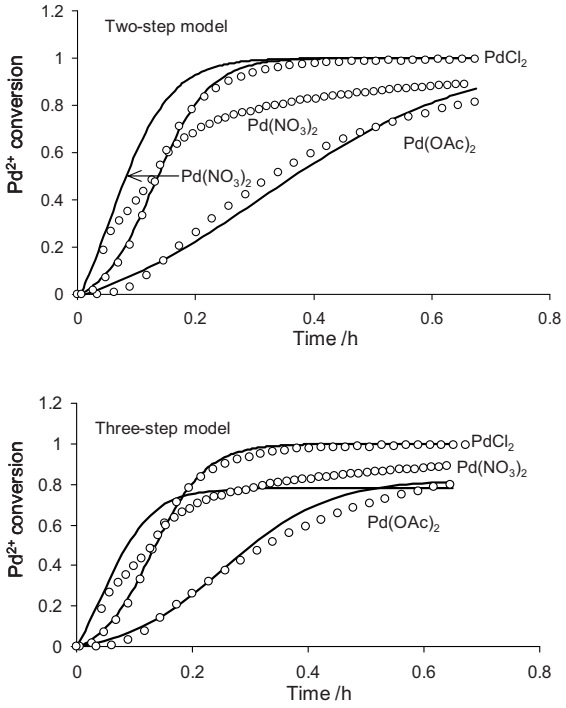

Figure 8. Experimental conversion profiles ('○' symbols, all measurements were performed in triplicate) of Pd^{2+}, using $PdCl_2$, $Pd(OAc)_2$, and $Pd(NO_3)_2$ as precursors and TOAF as reducing and stabilising agent, and corresponding simulated profiles (continuous curves) obtained from the two-step model (top) and the three-step model (bottom). Reaction conditions: 2 mL of 0.5 mM of PdX_2 precursor, 0.05 mL of 100 mM TOAF, 65 °C, dry N_2 atmosphere, magnetic stirring.

Table 2. Model rate constants for the different Pd precursors and TOAF

Precursor	k_1 (h^{-1})	k_2 ($10^4 M^{-1}h^{-1}$)	k_3 ($10^4 M^{-1}h^{-1}$)
$PdCl_2$	1.20	4.10	0.15
$Pd(OAc)_2$	0.40	2.20	5.10
$Pd(NO_3)_2$	4.00	3.00	1.20

For the aggregation process, $k_{3,acetate} > k_{3,chloride}$. Chloride ions are known to have a higher affinity for palladium than acetate ions,[49] thus we would expect less stabilising and more aggregation in the latter case. Although we cannot model the entire curve for the nitrate precursor, the initial rate for nitrate is higher than that of acetate or chloride. This

may reflect the tendency of $PdCl_2$ and $Pd(OAc)_2$ for forming dimeric and oligomeric species in solution.

Conclusions

The NAS/PCA approach can be used to extract quantitative concentration profiles of ion reduction and cluster formation for various Pd(II) salts and reducing/stabilising agents. This enables the quantitative monitoring of Pd clustering using simple UV-visible spectroscopy. Specific calibration models for each precursor/reducing agent combination should be used. Although we cannot directly measure the clustering rates, we can fit a model to overall reaction profiles. The kinetics of cluster formation fit to a simplified three-step model, including a slow nucleation step followed by autocatalytic surface growth and aggregation. The surface growth and aggregation steps are strongly influenced by the precursor counterions.

References

[1] L. Carrette, K. A. Friedrich, U. Stimming, *ChemPhysChem* **2000**, *1*, 162.

[2] A. Stanislaus, B. H. Cooper, *Catal. Rev. Sci. & Engg.* **1994**, *36*, 75.

[3] H.-U. Blaser, A. Indolese, F. Naud, U. Nettekoven, A. Schnyder, *Adv. Synth. Catal.* **2004**, *346*, 1583.

[4] E. Burello, D. Farrusseng, G. Rothenberg, *Adv. Synth. Catal.* **2004**, *346*, 1844.

[5] M. T. Reetz, J. G. de Vries, *Chem. Commun.* **2004**, 1559.

[6] M. Moreno-Mañas, R. Pleixats, *Acc. Chem. Res.* **2003**, *36*, 638.

[7] J. D. Aiken III, R. G. Finke, *J. Mol. Catal. A: Chem.* **1999**, *145*, 1.

[8] M. B. Thathagar, J. E. ten Elshof, G. Rothenberg, *Angew. Chem. Int. Ed.* **2006**, *45*, 2886.

[9] For recent reviews on cluster catalysis see (a) J. A. Widegren and R. G. Finke, *J. Mol. Catal. A: Chem.* 2003, **198**, 317; (b) B. L. Cushing, V. L. Kolesnichenko and C. J. O'Connor, *Chem. Rev.* 2004, **104**, 3893; (c) C. Burda, X. Chen, R. Narayanan and M. A. El-Sayed, *Chem. Rev*. 2005, **105**, 1025; (d) A. Biffis, M. Zecca and M. Basato, *J. Mol. Catal. A: Chem.* 2001, **173**, 249.

[10] T. Teranishi, M. Miyake, *Chem. Mater.* **1998**, *10*, 594.

[11] J. M. Petroski, Z. L. Wang, T. C. Green, M. A. El-Sayed, *J. Phys. Chem. B* **1998**, *102*, 3316.

[12] M. T. Reetz, M. Maase, *Adv. Mater.* **1999**, *11*, 773.

[13] S. King, K. Hyunh, R. Tannenbaum, *J. Phys. Chem. B* **2003**, *107*, 12097.

[14] P. Mulvaney, *Langmuir* **1996**, *12*, 788.

[15] J. A. Creighton, D. G. Eadon, *J. Chem. Soc., Farad. Trans.* **1991**, *87*, 3881.

[16] A. E. Saunders, M. B. Sigman, Jr., B. A. Korgel, *J. Phys. Chem. B* **2004**, *108*, 193.

[17] R. Tannenbaum, *Langmuir* **1997**, *13*, 5056.

[18] P. K. Sudeep, P. V. Kamat, *Chem. Mater.* **2005**, *17*, 5404.

[19] A. Henglein, M. Giersig, *J. Phys. Chem. B* **2000**, *104*, 6767.

[20] S. Oezkar, R. G. Finke, *J. Am. Chem. Soc.* **2002**, *124*, 5796.

[21] B. J. Hornstein, R. G. Finke, *Chem. Mater.* **2004**, *16*, 139.

[22] C. Besson, E. E. Finney, R. G. Finke, *Chem. Mater.* **2005**, *17*, 4925.

[23] C. Besson, E. E. Finney, R. G. Finke, *J. Am. Chem. Soc.* **2005**, *127*, 8179.

[24] J. D. Aiken III, R. G. Finke, *J. Am. Chem. Soc.* **1998**, *120*, 9545.

[25] J. Wang, H. F. M. Boelens, M. B. Thathagar, G. Rothenberg, *ChemPhysChem* **2004**, *5*, 93.

[26] J. D. Aiken III, Y. Lin, R. G. Finke, *J. Mol. Catal. A: Chem.* **1996**, *114*, 29.

[27] M. B. Thathagar, J. Beckers, G. Rothenberg, *J. Am. Chem. Soc.* **2002**, *124*, 11858.

[28] Matlab^{TM} version 6.1 is available from Mathworks, Natick USA.

[29] M. T. Reetz, W. Helbig, *J. Am. Chem. Soc.* **1994**, *116*, 7401.

[30] H. Bönnemann, G. Braun, W. Brijoux, R. Brinkmann, A. S. Tilling, K. Seevogel, K. Siepen, *J. Organomet. Chem.* **1996**, *520*, 143.

[31] H. Bönnemann, R. M. Richards, *Eur. J. Inorg. Chem.* **2001**, 2455.

[32] H. Wiener, J. Blum, H. Feilchenfeld, Y. Sasson, N. Zalmanov, *J. Catal.* **1998**, *110*, 184.

[33] S. Link, M. A. El-Sayed, *J. Phys. Chem. B* **1999**, *103*, 8410.

[34] F. Goettmann, A. Moores, C. Boissière, P. Le Floch, C. Sanchez, *Small* **2005**, *1*, 636.

[35] J. D. Aiken III, Y. Lin, R. G. Finke, *J. Mol. Catal. A: Chem.* **1996**, *114*, 29.

[36] G. Schmid, *Clusters and colloids: From theory to application*, VCH, Weinheim, **1994**.

[37] M. Tromp, J. R. A. Sietsma, J. A. van Bokhoven, G. P. F. van Strijdonck, R. J. van Haaren, A. M. J. van der Eerden, P. W. N. M. van Leeuwen, D. C. Koningsberger, *Chem. Commun.* **2003**, 128.

[38] Particles were counted using the imageJ software, available free of charge from http://rsb.info.nih.gov/ij/.

[39] J. S. Bradley, B. Tesche, W. Busser, M. Maase, M. T. Reetz, *J. Am. Chem. Soc.* **2000**, *122*, 4631.

[40] H. F. M. Boelens, W. T. Kok, O. E. de Noord, A. K. Smilde, *Anal. Chem.* **2004**, *76*, 2656.

[41] S. C. Cruz, P. J. Aarnoutse, G. Rothenberg, J. A. Westerhuis, A. K. Smilde, A. Bliek, *Phys. Chem. Chem. Phys.* **2003**, *5*, 4455.

[42] M. T. Reetz, W. Helbig, S. A. Quaiser, U. Stimming, N. Breuer, R. Vogel, *Science* **1995**, *267*, 367.

[43] S. C. Cruz, G. Rothenberg, J. A. Westerhuis, A. K. Smilde, *Anal. Chem.* **2005**, *77*, 2227.

[44] J. P. Wilcoxon, R. L. Williamson, R. Baughman, *J. Chem. Phys.* **1993**, *98*, 9933.

[45] M. A. Watzky, R. G. Finke, *J. Am. Chem. Soc.* **1997**, *119*, 10382.

[46] S. Bucher, J. Hormes, H. Modrow, R. Brinkmann, N. Waldofner, H. Bönnemann, L. Beuermann, S. Krischok, W. Maus-Friedrichs, V. Kempter, *Surf. Sci.* **2002**, *497*, 321.

[47] A. Roucoux, J. Schulz, H. Patin, *Chem. Rev.* **2002**, *102*, 3757.

[48] J. O. Bockris, A. K. N. Reddy, *Modern Electrochemistry, Vol. 1*, Plenum Press, London, **1976**.

[49] C. Amatore, E. Carre, A. Jutand, M. A. M'Barki, G. Meyer, *Organometallics* **1995**, *14*, 5605.